PNAS RESEARCH ARTICLE | MICROBIOLOGY

Epstein–Barr virus latency programs dynamically sensitize B cells to ferroptosis

Eric M. Burton[a,b,c], Jewel Voyer[a], and Benjamin E. Gewurz[a,b,c,d,1]

Edited by Thomas Shenk, Princeton University, Princeton, NJ; received October 6, 2021; accepted January 14, 2022

Epstein–Barr virus (EBV) causes 200,000 cancers annually. Upon B cell infection, EBV induces lipid metabolism to support B cell proliferation. Yet, little is known about how latent EBV infection, or human B cell stimulation more generally, alter sensitivity to ferroptosis, a nonapoptotic form of programmed cell death driven by iron-dependent lipid peroxidation and membrane damage. To gain insights, we analyzed lipid reactive oxygen species (ROS) levels and ferroptosis vulnerability in primary human CD19+ B cells infected by EBV or stimulated by key B cell receptors. Prior to the first mitosis, EBV-infected cells were exquisitely sensitive to blockade of glutathione biosynthesis, a phenomenon not observed with B cell receptor stimulation. Subsequently, EBV-mediated Burkitt-like hyperproliferation generated elevated levels of lipid ROS, which necessitated SLC7A11-mediated cystine import and glutathione peroxidase 4 (GPX4) activity to prevent ferroptosis. By comparison, B cells were sensitized to ferroptosis induction by combinatorial CD40-ligand and interleukin-4 stimulation or anti–B cell receptor and Toll-like receptor 9 stimulation upon GPX4 inhibition but not with SLC7A11 blockade. EBV transforming B cells became progressively resistant to ferroptosis induction upon switching to the latency III program and lymphoblastoid physiology. Similarly, latency I Burkitt cells were particularly vulnerable to blockade of SLC7A11 or GPX4 or cystine withdrawal, while latency III Burkitt and lymphoblastoid cells were comparatively resistant. The selenocysteine biosynthesis kinase PSTK was newly implicated as a cellular target for ferroptosis induction including in Burkitt cells, likely due to roles in GPX4 biosynthesis. These results highlight ferroptosis as an intriguing therapeutic target for the prevention or treatment of particular EBV-driven B cell malignancies.

lipid metabolism | tumor virus | ferroptosis | oxidative stress | B lymphocyte

Significance

Epstein–Barr virus (EBV) contributes to Burkitt lymphoma and post-transplant lymphoproliferative disease (PTLD). EBV-transforming programs activate lipid metabolism to convert B cells into immortalized lymphoblastoid cell lines (LCL), a PTLD model. We found that stages of EBV transformation generate lipid reactive oxygen species (ROS) byproducts to varying degrees, and that a Burkitt-like phase of B cell outgrowth requires lipid ROS detoxification by glutathione peroxidase 4 and its cofactor glutathione. Perturbation of this redox defense in early stages of transformation or in Burkitt cells triggered ferroptosis, a programmed cell death pathway. LCLs were less dependent on this defense, a distinction tied to EBV latency programs. This highlights ferroptosis induction as a potential therapeutic approach for prevention or treatment of certain EBV+ lymphomas.

Epstein–Barr virus (EBV) is an oncogenic γ-herpesvirus that persistently infects over 95% of adults worldwide. Although typically benign, EBV contributes to >200,000 cancers/year, including endemic Burkitt, Hodgkin, and non-Hodgkin lymphomas (1–3). The latter include central nervous system (CNS) lymphomas in people with advance HIV infection and post-transplant lymphoproliferative diseases (PTLD). EBV is also associated with nasopharyngeal and gastric carcinoma (4–6).

EBV infects tonsillar B cells and uses a series of latency programs to then navigate the B cell compartment in which different combinations of Epstein–Barr nuclear antigens (EBNA) and latent membrane proteins (LMP) are expressed (7, 8). In vitro, EBV converts resting B cells into immortalized lymphoblasts through a series of viral latency programs (5, 7). Over the first several days postinfection, the EBV prelatency program is expressed in which EBNA2 drives particularly high levels of the MYC proto-oncogene (9–12). Over this stage of infection, B cells quadruple in volume as they remodel but do not yet divide (13, 14). Over days 4 to 7 postinfection, cells express latency IIb, comprised of EBNA1, 2A and LP, and noncoding RNAs (14). Latency IIb–driven cells have elevated MYC levels and undergo Burkitt-like hyperproliferation (13, 15). Aberrant MYC expression is also a hallmark of Burkitt lymphoma, driven by chromosomal translocations between the *MYC* and immunoglobulin loci (16, 17).

EBV-infected B cells transition to lymphoblastoid physiology at approximately 1 wk postinfection and begin to express latency III comprised of six EBNA and two latent membrane proteins (LMP) (18). LMP1 mimics signaling by CD40, a key B cell coreceptor activated by T cell CD40-ligand (CD40L) (19–22). LMP2A mimics aspects of B cell receptor signaling (23, 24). Decreasing MYC levels and likely also feedback regulation enable steadily increasing LMP1 levels over the first weeks of the lymphoblastoid phase (25). Infected cells can then be grown as immortalized lymphoblastoid cell lines (LCL), which model PTLD and CNS lymphomas, which express the EBV latency III program.

EBNA2 and MYC strongly induce host lipid metabolism (12, 15). LMP1 also induces fatty acid synthesis enzymes at later timepoints (26). EBV-induced enzymes

Author contributions: E.M.B. and B.E.G. designed research; E.M.B. and J.V. performed research; E.M.B. and B.E.G. analyzed data; and E.M.B. and B.E.G. wrote the paper.

The authors declare no competing interest.

This article is a PNAS Direct Submission.

[1]To whom correspondence may be addressed. Email: bgewurz@bwh.harvard.edu.

This article contains supporting information online at http://www.pnas.org/lookup/suppl/doi:10.1073/pnas.2118300119/-/DCSupplemental.

Published March 11, 2022.

contribute to the biosynthesis of membrane phospholipid polyunsaturated fatty acids, which are implicated in ferroptosis (27). We therefore hypothesized that the pronounced increase in lipid metabolism, together with EBV-driven induction of oxidative phosphorylation reactive oxidative species (ROS) (12, 28, 29), sensitizes newly infected B cells to ferroptosis. The recently identified nonapoptotic ferroptosis programmed cell death pathway is driven by iron-catalyzed lipid ROS, which causes irreversible membrane peroxidation (30–32). Ferroptosis sensitivity is tightly linked to amino acid metabolism, particularly of cysteine, whose availability is limiting for the biosynthesis of the major cellular antioxidant glutathione (33). Most extracellular cysteine exists in the oxidized cystine state. Therefore, cells often import cystine via the SLC7A11/xCT transporter and then reduce it to cysteine or synthesize cysteine via the methionine metabolism transsulfuration pathway. The enzyme glutathione peroxidase 4 (GPX4) protects cells against oxidative stress by utilizing reduced glutathione (GSH) as the main reductant to resolve lipid ROS into alcohols (32).

Ferroptosis has been studied across a range of human cancer models, which show variable sensitivity to its induction (27, 34). However, effects of EBV or other tumor viruses on lipid ROS production and ferroptosis sensitization have not been studied. Likewise, effects of human primary B cell stimulation by physiological agonists such as CD40L, cytokine stimulation, B cell immunoglobulin receptor cross-linking, or Toll-like receptor (TLR) activation are uncharacterized. Here, we investigated lipid ROS and ferroptosis sensitivity across a time course of primary B cell immortalization by EBV, by B cell receptor activation, and in EBV-transformed Burkitt and lymphoblastoid B cells.

Results

EBV or Receptor Stimulation Promote Primary B Cell Lipid Peroxidation. We hypothesized that EBV-induced lipid metabolism sensitizes newly infected B cells to ferroptosis-inducing agents. To investigate this possibility, we purified primary human CD19+ peripheral blood B cells by negative selection. B cells were then infected by the EBV B95.8 strain at a multiplicity of infection of 0.1. We measured lipid ROS levels in uninfected cells and at 8 time points post-EBV infection that span B cell transformation into LCLs (Fig. 1*A*) using fluorescence-activated cell sorting (FACS) analysis of the lipid peroxidation sensor dye BODIPY-C11. EBV triggered lipid ROS production within the first 2 d of infection, which substantially increased upon entry into Burkitt-like hyperproliferation between days 4 to 7 postinfection. Lipid ROS levels remained elevated but progressively declined as cells converted to the lymphoblastoid phase (Fig. 1*B*).

To place the above EBV effects in a broader B cell context, we next stimulated primary B cells by key activation pathways: CD40, interleukin 4 (IL-4), B cell immunoglobulin cross-linking (αIgM), or toll receptor 9 (TLR9). Notably, T cells can activate B cells through CD40L+IL-4 costimulation, whereas gain-of-function CD79 and MyD88 mutations downstream of surface immunoglobulin and TLR9 often co-occur in diffuse large B cell lymphoma (35) (Fig. 1*C*). After 96 h of stimulation, lipid ROS levels were provoked by CpG, and to a somewhat lesser extent by CD40L, but not by IL-4 or αIgM treatment alone. Combinatorial CD40L+IL-4 or αIgM+CpG treatment did not induce levels beyond those seen with CD40L or CpG alone (Fig. 1*D*). To gain insights into how these stimuli might differentially affect lipid ROS levels in responding nondividing versus proliferating cells, primary B cells were labeled by CellTrace Violet and stimulated by individual or combinatorial receptor agonists for 4 d. Proliferation was monitored by FACS dye dilution assay. As expected, stimulation by CD40L, IL-4, αIgM, or CpG alone did not trigger robust proliferation responses, but did increase lipid ROS in the small population of proliferating cells. By contrast, cells proliferating in response to αIgM/CpG and to CD40/IL-4 had only modestly elevated lipid ROS levels as compared to the nondividing population. These results suggest that combinatorial stimuli may buffer increases in lipid ROS levels in the proliferating cell population to facilitate outgrowth (*SI Appendix*, Fig. S1 *A* and *B*) and that EBV may not trigger higher lipid ROS levels than physiological B cell activation.

EBV Dynamically Sensitizes B Cells to Ferroptosis. Erastin is a highly selective SLC7A11 inhibitor (36) that induces lipid ROS and ferroptosis by restricting the supply of cysteine, the rate-limiting component of glutathione biosynthesis (Fig. 2*A*). While erastin did not alter resting human CD19+ B cell lipid ROS or viability (*SI Appendix*, Fig. S1 *C*–*E*), EBV sensitized B cells to erastin-induced death at 2 d postinfection, as judged by the uptake of the vital dye 7-aminoactinomycin D (7-AAD) (Fig. 2*B*). Erastin sensitivity was greatest over the first week postinfection, with as many as >60% of cells positive for 7-AAD at day 7. Erastin-mediated cell death could be blocked by coadministration of the lipophilic antioxidant ferrostatin-1 (Fer-1), which scavenges lipid ROS (37). These results suggest that erastin induced ferroptosis in newly EBV-infected B cells (Fig. 2*B*).

Erastin sensitivity progressively diminished as EBV-infected cells converted to lymphoblastoid physiology (Fig. 2*B* and *SI Appendix*, Fig. S1*F*) and expressed increasing levels of LMP1 (25). By contrast, stimulation by the panel of B cell agonists, including combinatorial CD40+IL-4 and αIgM+CpG stimuli, failed to sensitize B cells to erastin despite increasing lipid ROS levels (Figs. 1*D* and 2*C* and *SI Appendix*, Fig. S1*G*). These results suggest that B cell activation by EBV versus immune receptor stimuli may trigger different routes of cysteine acquisition.

Whether primary human B cells are sensitive to GPX4 loss or ferroptosis is not known. Murine follicular B cells are not dependent on GPX4 for growth or survival, whereas marginal zone and B-1 B cells display elevated levels of lipid metabolism and require GPX4 to prevent lipid peroxidation and ferroptosis in vivo (38). We therefore asked if EBV infection, or B cell immunoreceptor stimulation more generally, confer GPX4 dependency on human B cells. Peripheral blood CD19+ B cells were EBV infected or stimulated by a range of B cell stimuli and then challenged with ML-210, a potent and selective GPX4 antagonist (Fig. 2*A*) (39). Resting B cells were not affected by ML-210 treatment (*SI Appendix*, Fig. S1 *C*–*D*). However, EBV-infected B cells were vulnerable to ML-210 across the transformation time course, reaching levels of nearly 100% 7-AAD positivity at day 7 postinfection, the time point with the greatest lipid ROS level (Figs. 1*B* and 2*D* and *SI Appendix*, Fig. S2*A*). Importantly, fer-1 treatment rescued ML-210–induced cell death, supporting on-target ML-210 effects on the ferroptosis pathway. Despite similarly robust lipid ROS induction by CpG stimulation (Fig. 1*D*), ML-210 more robustly induced ferroptosis in cells stimulated by combinatorial CD40L+IL-4 or by αIgM+CpG as judged by the fold change of 7AAD+ cells from control- or Fer-1–treated cell levels (Fig. 2*E* and *SI Appendix*, Fig. S2*B*). These data suggest that the route of B cell stimulation is a major determinant of ferroptosis vulnerability and that human peripheral blood B

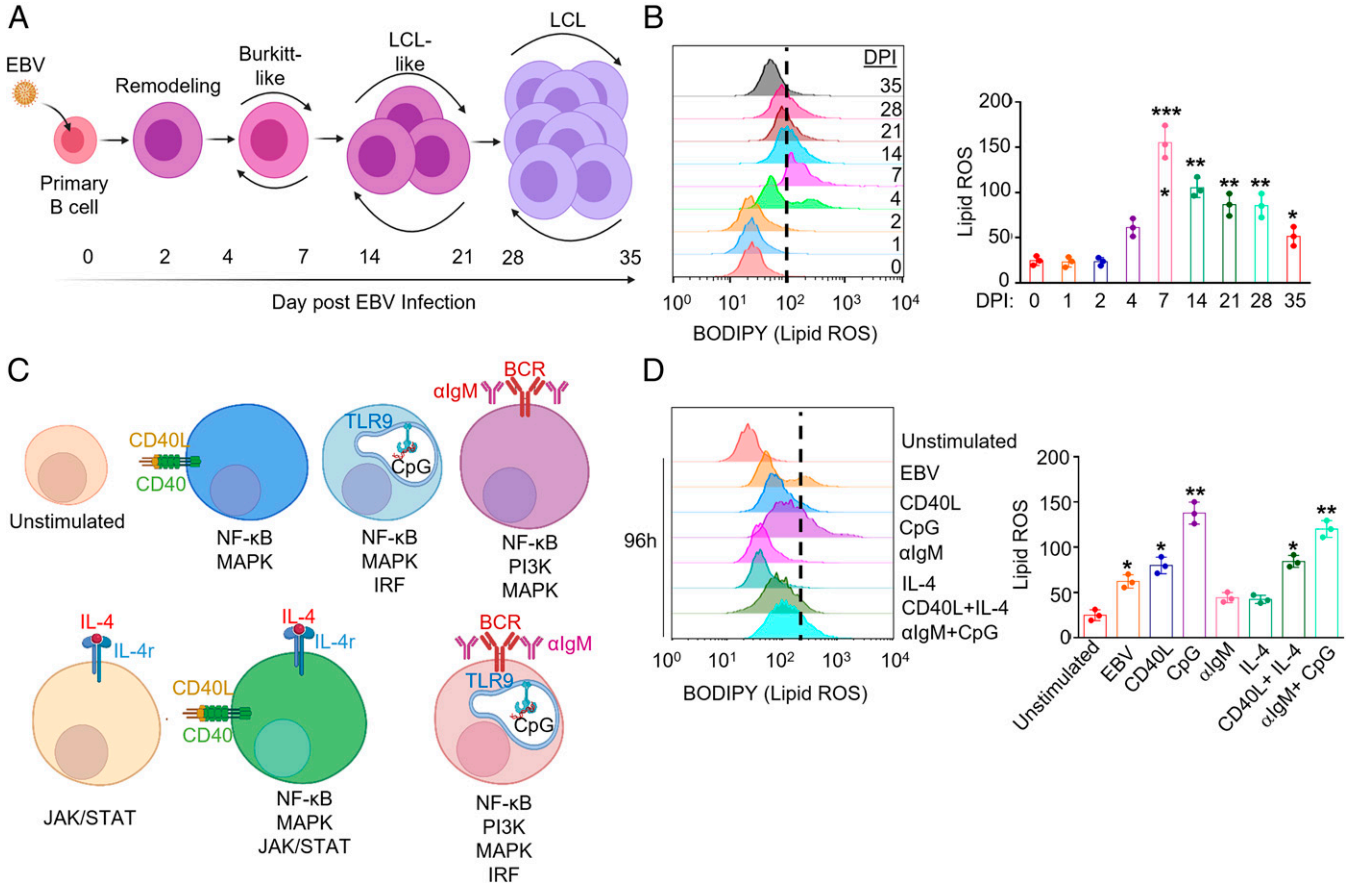

Fig. 1. B cell EBV infection and immune receptor stimulation trigger varying levels of lipid ROS. (*A*) Model of the stages of EBV-mediated B cell transformation into LCLs. (*B*) Representative FACS histograms of primary B cell BODIPY (lipid ROS) levels at the indicated day post-EBV infection (DPI). Shown at *Right* are the mean fluorescence intensity (MFI) + SD of lipid ROS levels from $n = 3$ independent replicates. (*C*) Model of agonists used to stimulate primary B cells. Key pathways activated by each mode of stimulation are shown beneath each cell model. (*D*) Representative FACS histograms of primary B cell BODIPY (lipid ROS) levels at day 4 of the indicated stimulation: Mega-CD40L (50 ng/mL), αIgM (1 μg/mL), CpG (1 μM), or IL-4 (20 ng/mL). Day 0 unstimulated cells were included for reference. Shown at *Right* are the BODIPY MFI + SD values from $n = 3$ independent replicates. *P* values were determined by one-sided Fisher's exact test. $*P < 0.05$, $**P < 0.005$, $***P < 0.0005$.

cells require GPX4 upon EBV infection or with combinatorial B cell receptor activation.

EBV+ Latency I Burkitt Cells Are More Vulnerable to Ferroptosis Than Latency III LCLs. We next asked whether similar relationships could be observed in EBV-transformed B cells with distinct latency states. Burkitt lymphoma (BL) is driven by aberrant MYC expression, reminiscent of newly infected cells over the first several days of infection (16). Erastin significantly increased lipid ROS and 7-AAD uptake in EBV+ Daudi BL cells but not in the LCL GM12879 (Fig. 3 *A* and *B* and *SI Appendix*, Fig. S3 *A* and *B*). Fer-1 blocked erastin-induced lipid ROS and cell death, suggesting on-target effects on ferroptosis induction in Daudi cells. In further support, CRISPR/Cas9 *SLC7A11* knockout (KO) significantly reduced viable cell numbers in Daudi but not GM12878 LCLs, which could be rescued by Fer-1 (Fig. 3 *C* and *D* and *SI Appendix*, Table S1). Similar results were observed in another BL/LCL pair (*SI Appendix*, Fig. S3 *A–F*). These results suggest that Burkitt cells are significantly more dependent than LCLs on cystine uptake via SLC7A11 to support redox defense.

We next tested whether BLs and LCLs were dependent on GPX4 for ferroptosis resistance. Interestingly, GPX4 inactivation by ML-210 strongly induced lipid ROS and cell death in Daudi BL but to a lesser extent in GM12879 LCLs. These phenotypes were rescued by Fer-1, suggestive of on-target effects on lipid ROS and ferroptosis (Fig. 3 *E* and *F* and *SI Appendix*, Fig. S4 *A* and *B*). Similar results were obtained in a second BL/LCL pair (*SI Appendix*, Fig. S4 *C* and *D*). CRISPR *GPX4* editing by independent single guide RNAs also significantly reduced BL cell survival to a somewhat greater extent than LCLs in a manner rescuable by Fer-1 (Fig. 3 *G* and *H* and *SI Appendix*, Table S1 and Fig. S4 *E* and *F*).

GPX4 utilizes selenocysteine as a component of its catalytic triad (40). Interrogation of Cancer Dependency Map CRISPR data from >700 cell lines (41) demonstrated a particularly strong codependency between GPX4 and the kinase phosphoseryl transfer RNA (tRNA) kinase (PSTK) (*SI Appendix*, Fig. S4 *G*). PSTK phosphorylates seryl-tRNA(Sec) in order to yield O-phosphoseryltRNA(Sec), an activated intermediate used in selenocysteine biosynthesis (42). Since this kinase has not previously been studied in the context of ferroptosis or in EBV-infected cells, we used CRISPR to test effects of PSTK KO. We found that PSTK and GPX4 KO exhibited similar phenotypes, with more robust effects on BL than LCL survival (Fig. 3 *I* and *J* and *SI Appendix*, Table S1 and Fig. S4 *H* and *I*). Intriguingly, CRISPR PSTK depletion also reduced GPX4 steady state levels, suggesting a potential PSTK role in GPX4 biosynthesis or stability (Fig. 3 *I* and *J* and *SI Appendix*, Fig. S4 *H* and *I*). Taken together, these data suggest that Burkitt cells, and to a lesser extent LCLs, are dependent on GPX4 for lipid

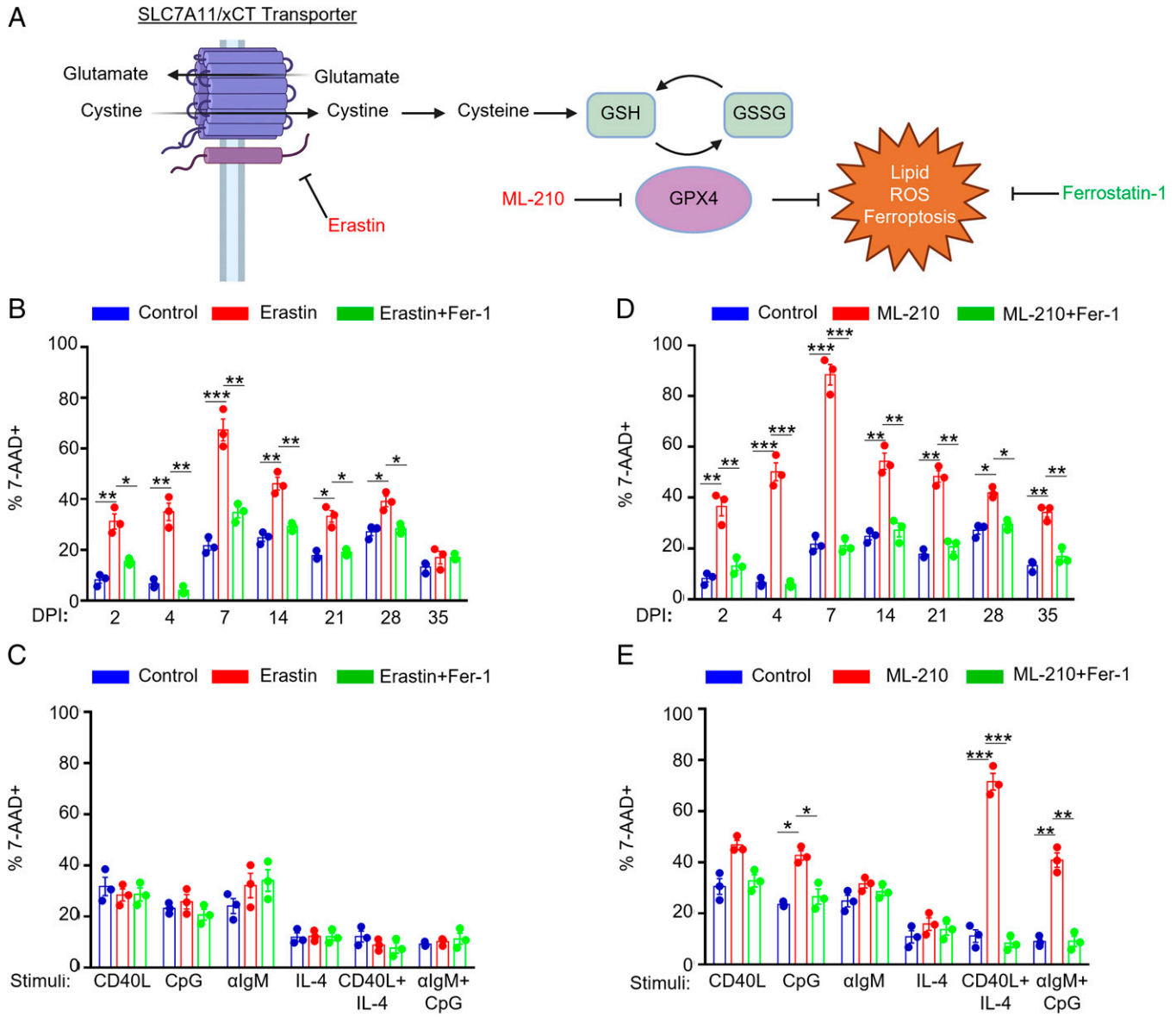

Fig. 2. Effects of EBV infection versus B cell receptor stimulation on sensitization to ferroptosis. (*A*) Model of erastin and ML-210 ferroptosis inducing agent mechanisms of action on ferroptosis induction. GSH, reduced glutathione. GSSG, oxidized glutathione. (*B*) FACS %7-AAD+ mean + SD values from $n = 3$ independent replicates of primary B cells from independent donors infected by EBV for the indicated day postinfection (DPI) and treated with 10 μM erastin and/or 5 μM Fer-1 for 24 h prior to analysis as indicated. (*C*) FACS %7-AAD+ mean + SD values from $n = 3$ independent replicates of primary B cells from independent donors stimulated as indicated by Mega-CD40L (50 ng/mL), αIgM (1 μg/mL), CpG (1 μM), or IL-4 (20 ng/mL) for 48 h and treated with 10 μM erastin and/or 5 μM Fer-1 for 24 h prior to analysis as indicated. (*D*) FACS %7-AAD+ mean + SD values from $n = 3$ independent replicates using primary B cells from independent donors infected by EBV for the indicated DPI and treated with 1 μM ML-210 and/or 5 μM Fer-1 for 24 h prior to analysis as indicated. (*E*) FACS %7-AAD+ mean + SD values from $n = 3$ independent replicates of primary B cells from independent donors stimulated as indicated for 48 h and treated with 1 μM ML-210 and/or 5 μM Fer-1 for 24 h prior to analysis as indicated. *P* values were determined by one-sided Fisher's exact test. $*P < 0.05$, $**P < 0.005$, $***P < 0.0005$.

ROS detoxification and ferroptosis defense and that PSTK is a potentially druggable ferroptosis pathway kinase target.

The EBV Latency III Induces Resistance to Ferroptosis-Inducing Agents. To gain insights into how EBV latency programs alter lipid ROS levels and ferroptosis vulnerability, we utilized isogenic Burkitt tumor–derived MUTU I versus III cell lines, which differ only by EBV latency I versus III programs (43). Lipid ROS levels were somewhat higher at baseline in MUTU III than in MUTU I (Fig. 4*A* and *SI Appendix*, Fig. S5*A*). Erastin treatment increased lipid ROS levels in both, although the fold change from baseline was higher in MUTU I (Fig. 4*A* and *SI Appendix*, Fig. S5*A*). Fer-1 restored baseline lipid ROS levels in erastin-treated MUTU I and III. Consistent with the higher fold change in lipid ROS levels seen in MUTU I, erastin also caused higher levels of cell death in MUTU I treated for 24 h, which could be rescued by Fer-1, indicative of ferroptosis (Fig. 4*B* and *SI Appendix*, Fig. S5*B*). ML-210 induced more lipid ROS in MUTU I than in MUTU III and induced higher levels of cell death, again rescuable by Fer-1 (Fig. 4 *C* and *D* and *SI Appendix*, Fig. S5 *C* and *D*). Latency III cell lines had substantially higher erastin and ML-210 half-maximal inhibitory concentration (IC_{50}) than latency I B cell lines (Fig. 4 *E*–*H*). For instance, the LCL Kem III had substantially higher erastin and ML-210 IC_{50} values than latency I Kem I BL cells cultured from the same tumor sample (44). This phenotype was evident in Burkitt cells harboring either of the two major EBV strain types, suggesting evolutionary conservation.

We next asked whether switching off the latency III program in an LCL and replacing it with conditional MYC overexpression

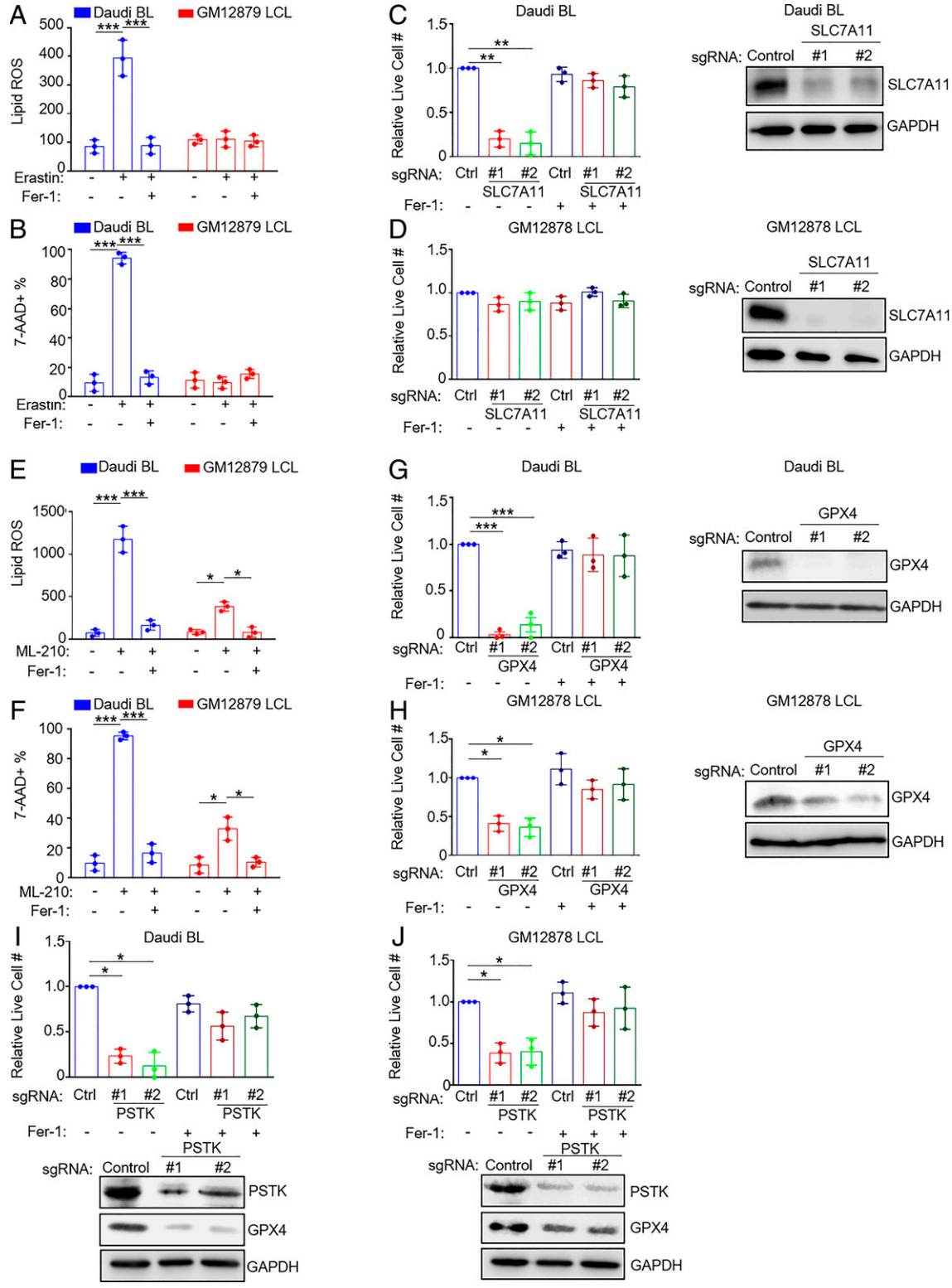

Fig. 3. EBV-infected BL cells are more susceptible to ferroptosis inducing agents than lymphoblastoid cell lines. (*A*) BODIPY mean fluorescence intensity (MFI) + SD values from $n = 3$ independent replicates of Daudi BL versus GM12879 LCLs treated with erastin (10 μM) for 18 h and measured by FACS. (*B*) %7-AAD+ mean + SD values from $n = 3$ replicates of Daudi and GM12879 cells treated with erastin (10 μM) for 24 h and measured by FACS. (*C* and *D*) Relative mean + SD live cell numbers from CellTiter-Glo analysis from $n = 3$ replicates of Cas9+ Daudi (*C*) versus GM12878 LCLs (*D*) after 7 d of control (ctrl) or independent SLC7A11 single guide RNA (sgRNA) expression in the absence or presence of 5 μM Fer-1 as indicated. Shown at *Right* are representative immunoblots of whole-cell lysates (WCL) for SLC7A11 or GAPDH load control. (*E*) BODIPY MFI + SD values from $n = 3$ independent replicates of Daudi BL versus GM12879 LCLs treated with ML-210 (1 μM) for 18 h. (*F*) 7-AAD+ mean + SD values from $n = 3$ replicates of Daudi and GM12879 cells treated with ML-210 (1 μM) for 24 h and measured by FACS. (*G* and *H*) Relative mean + SD live cell numbers from CellTiter-Glo analysis from $n = 3$ replicates of Cas9+ Daudi (*G*) versus GM12878 LCLs (*H*) after 7 d of ctrl or GPX4 sgRNA expression in the absence or presence of 5 μM Fer-1 as indicated. Shown at *Right* are representative immunoblots of WCL for GPX4 or GAPDH load control. (*I* and *J*) Relative mean + SD live cell numbers from CellTiter-Glo analysis from $n = 3$ replicates of Cas9+ Daudi (*I*) versus GM12878 LCLs (*J*) after 7 d of ctrl or PSTK sgRNA expression in the absence or presence of 5 μM Fer-1 as indicated. Shown at *Right* are representative immunoblots of WCL for PSTK or GAPDH load control. *P* values were determined by one-sided Fisher's exact test. $*P < 0.05$, $**P < 0.005$, $***P < 0.0005$.

in the context of latency I altered sensitivity to ferroptosis. We utilized the P493-6 LCL, which have conditional Tet-off MYC and 4hydroxytamoxifen (4HT)- activated EBNA2 alleles (45). P493-6 grown in 4HT and doxycycline grow as LCLs, whereas cells grown without either lose latency III and express high levels of MYC to simulate EBV+ BL cell physiology (45) (*SI Appendix*, Fig. S5*E*). P493-6 grown in the LCL state exhibited significantly higher erastin IC_{50} values (58.4 versus 6.7 μM) and likewise for ML-210 (1.2 versus 0.5 μM) (Fig. 4 *I* and *J*). These results suggest that MYC-driven lipid metabolism in newly EBV-infected and Burkitt cells induces dependency on SLC7A11 cystine import, glutathione biosynthesis, and GPX4-based ferroptosis defense.

Glutathione Biosynthesis Is Critical for Burkitt-Like and Burkitt Cell Survival. The enzyme glutamate-cysteine ligase (GCLC) catalyzes the rate-limiting step in glutathione biosynthesis, the production of γ-glutamylcysteine from cysteine and glutamate (Fig. 5*A*). Given the observed differences in EBV-infected cell sensitivity to the blockade of SLC7A11 or GPX4 as well as our prior observation that resting B cells have low levels of glutathione (12), we next asked whether newly EBV-infected cells are dependent on glutathione synthesis for survival. We treated CD19+ primary B cells at 7 time points postinfection with buthionine sulfoximine (BSO), a highly selective GCLC antagonist. We then monitored effects on 7-AAD uptake and lipid ROS levels. Unexpectedly, cells were exquisitely sensitive to BSO treatment at day 2 post-EBV infection, in which we observed highly elevated lipid ROS levels, and >80% underwent cell death (Fig. 5 *B* and *C* and *SI Appendix*, Fig. S6 *A* and *B*). Supplementation with either Fer-1 or GSH reduced lipid ROS and significantly rescued viability, suggesting that BSO induced ferroptosis at this early time point postinfection (Fig. 5 *B* and *C* and *SI Appendix*, Fig. S6 *A* and *B*). Surprisingly, we did not observe significant BSO-driven increases in lipid ROS or cell death at later times (Fig. 5 *A* and *B*). It is possible that BSO did not completely block GCLC activity at the dose used. Therefore, these results are consistent with a model in which particularly low GSH stores in resting B cells render cells particularly sensitive to GCLC inhibition at day 2 postinfection.

We next cross-compared BSO effects on resting or receptor-stimulated human B cells. BSO did not increase lipid ROS or death in resting B cells but strongly induced lipid ROS and 7-AAD uptake in cells stimulated for 2 d by CD40L+IL-4. Interestingly, these effects were not seen with αIgM+CpG stimulation (Fig. 5 *D* and *E* and *SI Appendix*, Fig. S6 *C* and *D*), suggesting that the route of primary B cell stimulation dictates dependency on GCLC enzymatic activity at early time points. To then measure effects on proliferation, B cells were labeled by carboxyfluorescein succinimidyl ester and infected by EBV or stimulated with CD40L+IL-4 or αIgM+CpG for 4 d. Proliferation was monitored by FACS dye dilution assay. BSO blocked proliferation of EBV-infected and CD40+IL-4–stimulated cells but only partially blocked αIgM+CpG-driven proliferation. BSO effects were rescued by reduced glutathione (GSH) but not Fer-1, suggesting glutathione roles beyond lipid ROS detoxification in support of B cell proliferation (Fig. 5*F*).

We next examined effects of BSO treatment on a panel of Burkitt versus LCLs. BSO significantly increased lipid ROS and 7-AAD uptake in EBV+ BLs but not LCLs (Fig. 5 *G* and *H* and *SI Appendix*, Fig. S6 *E* and *F*). Fer-1 or GSH supplementation rescued lipid ROS and suppressed BL cell death, indicating that BSO induced ferroptosis in these BL cells. To then examine a potential relationship between EBV latency program and glutathione synthesis, we used CRISPR to deplete GCLC (*SI Appendix*, Fig. S7*A* and Table S1). In agreement with our BSO data, *GCLC* editing markedly increased lipid ROS and cell death in P3HR-1 (Fig. 5 *I* and *J* and *SI Appendix*, Fig. S7 *B* and *C*). By contrast, GCLC depletion in Jijoye, the parental latency III cell line of P3HR-1, or in GM12878 LCLs had little effect on lipid ROS or survival (Fig. 5 *I* and *J*). Similar results were obtained with BSO treatment (*SI Appendix*, Fig. S7 *D*–*F*). These data suggest that latency III generates lower lipid ROS levels and utilizes distinct glutathione metabolism and/or compensatory mechanisms to control lipid ROS.

EBV-Infected and Stimulated Primary B Cells Are Addicted to Cystine. We next investigated whether EBV infection or B cell stimulation renders primary or EBV-transformed B cells auxotrophic for cystine (Fig. 6*A*). While cysteine is not an essential amino acid for many cell types and can be synthesized from methionine via the transsulfuration pathway, some cell states require cystine import to prevent ferroptosis (46). We therefore investigated the role of cystine restriction on B cell lipid ROS and ferroptosis. At each of seven time points post-EBV infection, cystine withdrawal induced B cell death as judged by 7-AAD uptake (Fig. 6*B*). Cell viability was significantly restored by addition of Fer-1, indicating that EBV-infected B cells require cystine to prevent ferroptosis induction. Similarly, GSH supplementation rescued cell death, perhaps as it can be metabolized extracellularly to provide cysteine. We next cross-compared effects of cystine restriction on B cells infected by EBV versus stimulated by CD40L+IL4 or αIgM+CpG for 4 d. In all cases, cystine withdrawal restrained B cell proliferation (Fig. 6*C*). GSH but not Fer-1 nearly completely rescued proliferation driven by EBV, αIgM+CpG, and by CD40L+IL-4 stimulation (Fig. 6*C*). Furthermore, whereas cystine withdrawal did not trigger lipid ROS or cell death in unstimulated B cells, it significantly elevated lipid ROS and 7-AAD uptake in CD40L+IL-4–stimulated cells and to a much lesser extent in αIgM+CpG–treated cells (Fig. 6 *D* and *E* and *SI Appendix*, Fig. S8*A*). These results suggest that lipid metabolism programs driven by EBV infection or CD40L+IL-4 stimulation necessitate a greater dependence on cystine uptake to buffer lipid ROS.

Finally, we investigated whether extracellular cystine had similarly important roles during EBV transformed B cell lipid ROS generation and ferroptosis defense. Cystine withdrawal significantly elevated lipid ROS levels and cell death in BL but not in either LCL over 24 h, rescued by Fer-1 or GSH (Fig. 6 *F* and *G* and *SI Appendix*, Fig. S8 *B* and *C*). While able to survive for longer periods of cystine withdrawal, cystine restriction ultimately triggered LCL death, similar to what we observed when culturing day 35 postinfection primary B cells in cystine-restricted media (Fig. 6 *B* and *H* and *SI Appendix*, Fig. S8*D*). These results are consistent with a model in which greater GSH stores enable LCLs to survive cystine withdrawal for longer periods of time than Burkitt cells. Given their resistance to even prolonged erastin treatment or SLC7A11 KO, these results also suggest that latency III cells have alternative means of meeting cysteine demand and further suggest that they may utilize non-GPX4 pathways for lipid ROS detoxification (Fig. 7).

Discussion

Vulnerability to ferroptosis is associated with numerous aspects of cellular physiology, including amino acid, iron, lipid, and NADPH metabolism (32). Murine marginal zone and B1 type

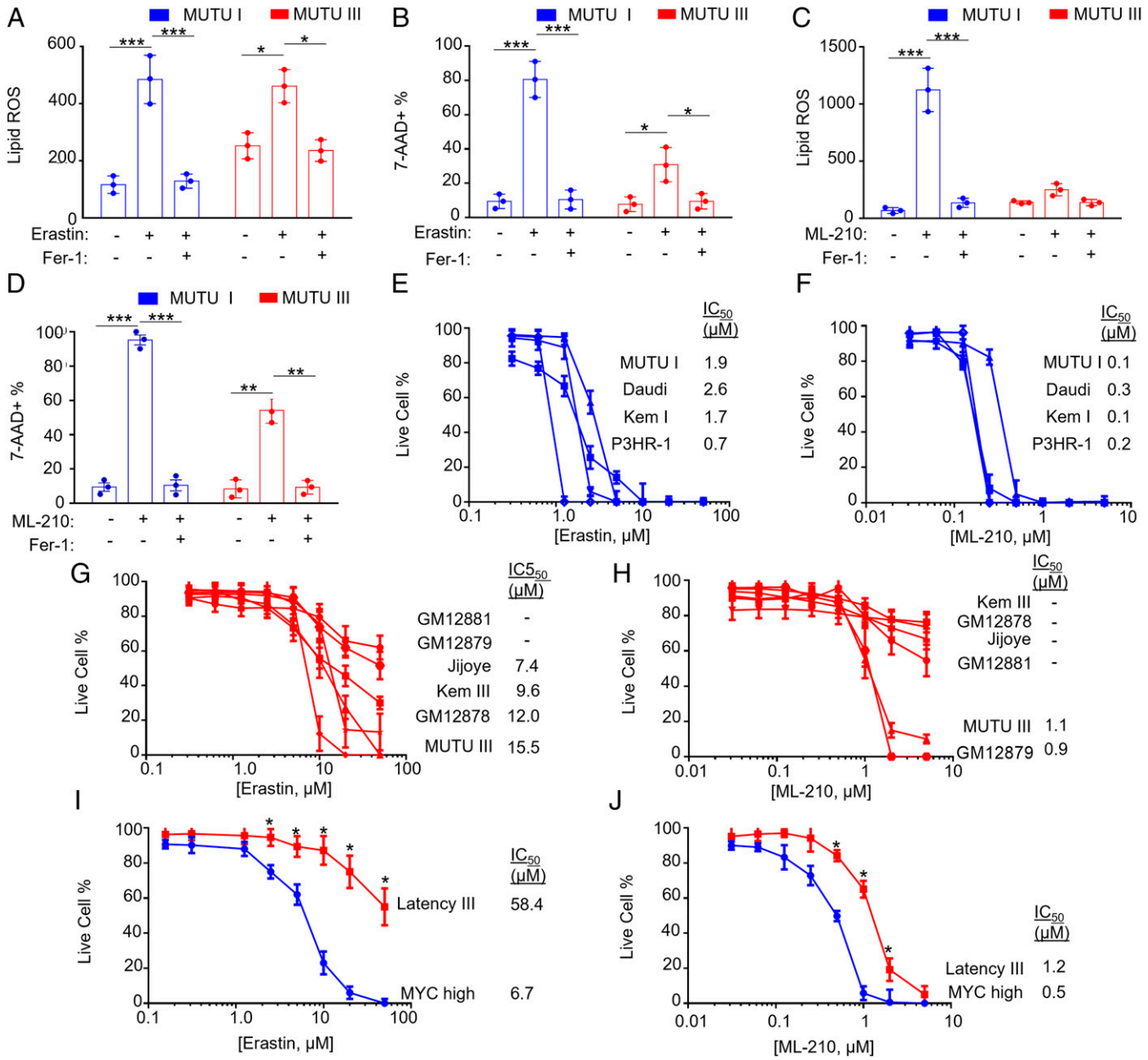

Fig. 4. The EBV latency III program confers resistance to ferroptosis-inducing agents. (*A*) BODIPY MFI + SD values from $n = 3$ independent replicates of MUTU I versus III BL cells treated with erastin (10 μM) and/or Fer-1 (5 μM) for 18 h and measured by FACS. (*B*) %7-AAD+ mean + SD values from $n = 3$ replicates of MUTU I versus III BL cells treated with erastin (10 μM) and/or Fer-1 (5 μM) for 24 h and measured by FACS. (*C*) BODIPY MFI + SD values measured by FACS of $n = 3$ independent replicates of MUTU I versus III BL cells treated with ML-210 (1 μM) and/or Fer-1 (5 μM) for 18 h as indicated. (*D*) %7-AAD+ mean + SD values measured by FACS of $n = 3$ replicates of MUTU I versus III BL cells treated with ML-210 (1 μM) and/or Fer-1 (5 μM) for 24 h and measured by FACS. (*E*) Dose–response curves of cells with EBV latency I to erastin for 24 h. Mean + SD of CellTiter-Glo live cell numbers from $n = 3$ replicates. IC_{50} values are shown at *Right*. (*F*) Dose–response curves of cells with EBV latency III to erastin for 24 h. Mean + SD of CellTiter-Glo live cell numbers from $n = 3$ replicates. IC_{50} values are shown at *Right*. (*G*) Dose–response curves of cells with EBV latency I to ML-210 for 24 h. Mean + SD of CellTiter-Glo live cell numbers from $n = 3$ replicates. IC_{50} values are shown at *Right*. (*H*) Dose–response curves of cells with EBV latency III to ML-210 for 24 h. Mean + SD of CellTiter-Glo live cell numbers from $n = 3$ replicates. IC_{50} values are shown at *Right*. (*I*) Dose–response curves of P-493 cells grown in the MYC-high Burkitt-like state (blue) or EBNA2-driven latency III state (red) to erastin for 24 h. Mean + SD of CellTiter-Glo live cell numbers from $n = 3$ replicates. IC_{50} values are shown at *Right*. (*J*) Dose–response curves of P-493 cells grown in the MYC-high Burkitt-like state (blue) or EBNA2-driven latency III state (red) to ML-210 for 24 h. Mean + SD of CellTiter-Glo live cell numbers from $n = 3$ replicates. IC_{50} values are shown at *Right*. *P* values were determined by one-sided Fisher's exact test. $*P < 0.05$, $**P < 0.005$, $***P < 0.0005$.

B cells require GPX4 to prevent ferroptosis, while murine follicular B cells do not, highlighting B cell differentiation specific roles (38). Notably, murine B cells have low levels of SLC7A11 expression and therefore require reducing agents such as β-mercaptoethanol or sulfhydryl-containing compounds to survive in vitro (47). Human B cells do not require the addition of these reducing agents and exhibited low levels of lipid ROS at baseline. How untransformed human B cells respond to lipid oxidative stress resulting from EBV oncogenic challenge, and how this cross-compares with B cell receptor–driven metabolic reprogramming, have remained important open questions. Here, we present evidence that latent EBV triggered lipid ROS production in newly infected primary human B cells, which induced vulnerability to ferroptosis-inducing agents at multiple

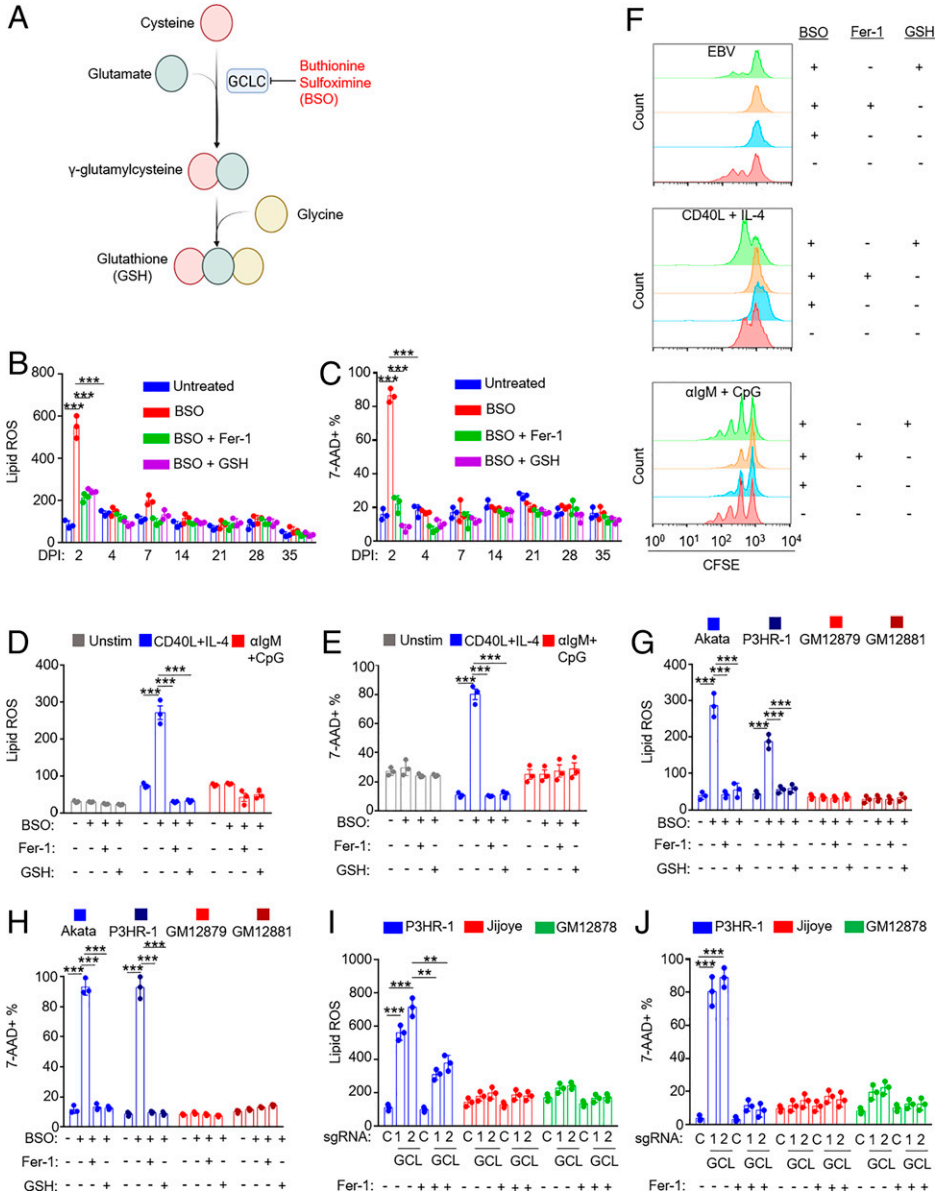

Fig. 5. Effects of glutathione synthesis inhibition on EBV-infected, receptor-stimulated, and EBV-transformed B cells. (*A*) Diagram of the glutathione synthesis pathway and its inhibition by BSO. (*B*) FACS BODIPY MFI + SD values from $n = 3$ replicates of primary B cells treated at the indicated day post-EBV infection with BSO (100 §M) and Fer-1 (5 μM) or 2.5 mM GSH for 72 h as indicated. (*C*) %7-AAD+ mean + SD values from $n = 3$ replicates of primary B cells treated at the indicated day post-EBV infection with BSO (100 §M) and Fer-1 (5 μM) or 2.5 mM GSH for 72 h as indicated. (*C*) FACS %7-AAD+ mean + SD values from $n = 3$ independent replicates of primary B cells from independent donors treated at indicated day post-EBV infection with BSO (100 §M) and Fer-1 (5 μM) or 2.5 mM GSH for 72 h as indicated. (*D*) FACS BODIPY MFI + SD values from $n = 3$ independent replicates of primary B cells from independent donors stimulated for 2 d by CD40L (50 ng/mL) and IL-4 (20 ng/mL) or αIgM (1 μg/mL) and CpG (1 μM) and then treated with BSO (100 μM), 5 μM Fer-1, or 2.5 mM GSH for 48 h prior to analysis as indicated. (*E*) FACS %7-AAD+ mean + SD values from $n = 3$ independent replicates of primary B cells from independent donors stimulated for 2 d by CD40L (50 ng/mL) and IL-4 (20 ng/mL) or αIgM (1 μg/mL) and CpG (1 μM) and then treated with BSO (100 μM), 5 μM Fer-1, or 2.5 mM GSH for 48 h prior to analysis as indicated. (*F*) FACS analysis of carboxyfluorescein succinimidyl ester–labeled primary B cells infected with EBV or treated with the indicated stimuli in the presence of BSO, Fer-1, or GSH, as indicated. After 4 d, proliferation was analyzed via FACS. Plot is representative of $n = 3$ independent replicates. (*G*) FACS BODIPY MFI + SD values from $n = 3$ independent replicates of EBV-Akata and EBV+ P3HR-1 BL or GM12879 and GM12881 LCLs treated with BSO (100 §M), Fer-1 (5 §M), or GSH (2.5 mM) for 48 h as indicated. (*H*) FACS %7-AAD+ mean + SD values from $n = 3$ independent replicates of EBV-Akata and EBV+ P3HR-1 BL or GM12879 and GM12881 LCLs treated with BSO (100 §M), Fer-1 (5 §M), or GSH (2.5 mM) for 72 h as indicated. (*I*). FACS BODIPY MFI + SD values from $n = 3$ independent replicates of Cas9+ latency I P3HR-1, latency III Jijoye, or GM12878 LCLs expressing control (c) or GCLC (GCL) sgRNAs for 12 d and treated with Fer-1 (5 §M), as indicated. (*J*) FACS %7-AAD+ mean + SD values from $n = 3$ independent replicates as in *I*, analyzed 14 d after single guide RNA expression. *P* values were determined by one-sided Fisher's exact test. $*P < 0.05$, $**P < 0.005$, $***P < 0.0005$.

times postinfection (Fig. 7). Likewise, we found that latency I Burkitt cells were exquisitely sensitive to ferroptosis induction, while latency III B-cells were more refractory (Fig. 7).

Metabolic reprogramming is required upon B cell challenge by EBV or by receptor-driven proliferation to meet anabolic demands (12, 48, 49). Yet, metabolic stress is a major barrier to EBV-mediated B cell transformation (28). Our results suggest that EBV must carefully balance highly induced anabolic lipid metabolism with ferroptosis defense, particularly at early time points postinfection and in Burkitt cells, which share hyperactive MYC states. Notably, resting human B cells and Burkitt cells also have very low levels of glutathione and glutathione synthesis (12) in contrast to many cellular environments where glutathione is present at millimolar quantities. To meet demand, we hypothesize that EBNA2 and MYC highly induce one-carbon metabolism, which supports glutathione biosynthesis via the production

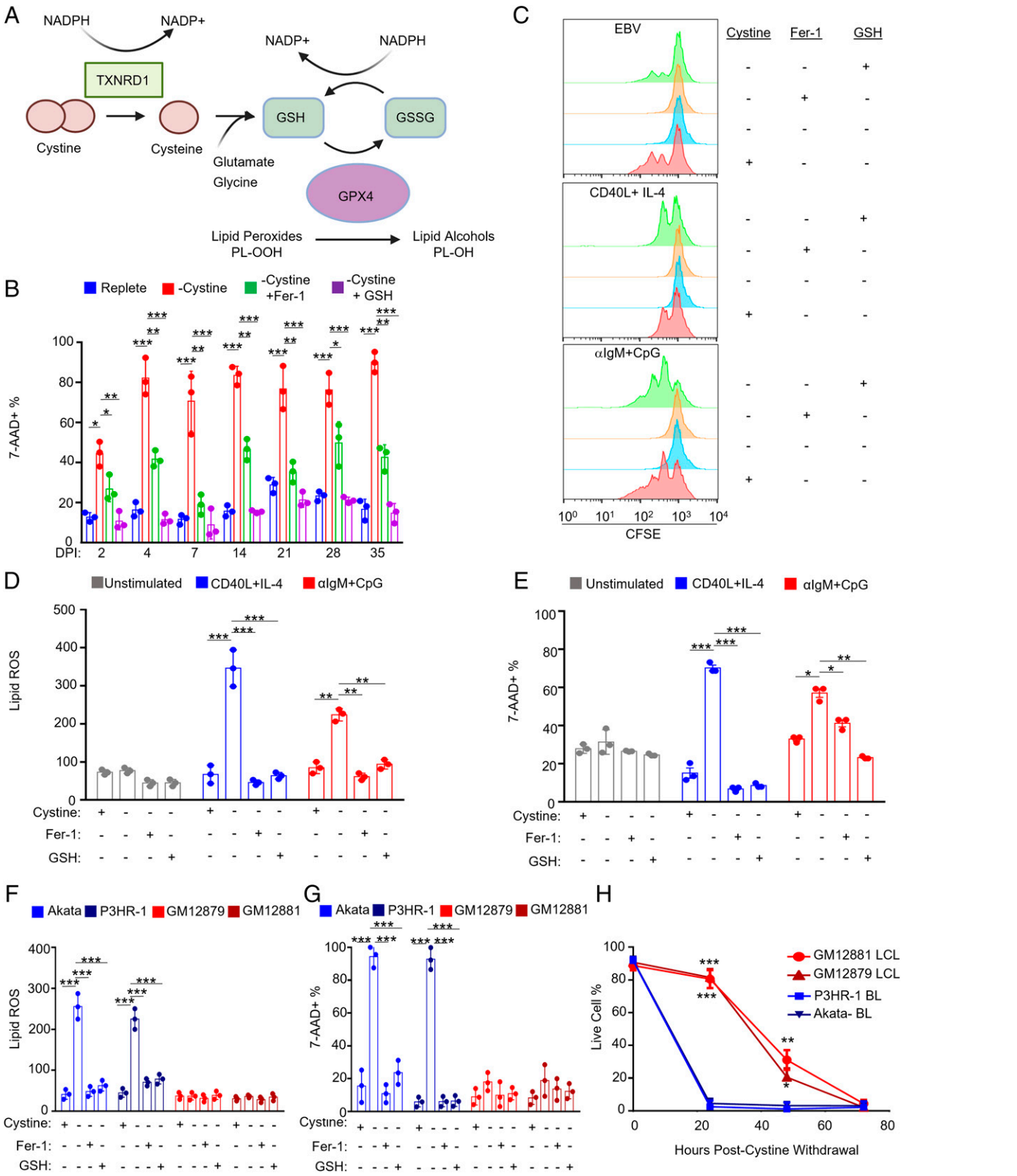

Fig. 6. EBV-infected cells are dependent on cystine for growth and survival. (*A*) Schematic of cystine and glutathione metabolism in control of lipid peroxidation. (*B*) FACS %7-AAD+ mean + SD values from $n = 3$ independent replicates of primary B cells infected with EBV for the indicated day postinfection (DPI), harvested, and seeded into media with or without cystine and treated with Fer-1 or GSH as indicated for 72 h. (*C*) FACS analysis of CFSE-labeled primary B cells infected with EBV or treated with the indicated stimuli in the presence of Fer-1 or GSH as indicated. After 4 d, proliferation was analyzed via FACS. Plot is representative of $n = 3$ independent replicates. (*D*) FACS BODIPY mean + SD values from $n = 3$ replicates of primary B cells unstimulated or treated with indicated stimuli for 48 h and then seeded into media with the same stimuli, with or without cystine, Fer-1 and GSH as indicated for 48 h. (*E*) FACS %7-AAD+ mean + SD values from $n = 3$ replicates of primary B cells as in *D* and seeded into media with or without cystine, Fer-1, and GSH as indicated for 72 h. (*F* and *G*) FACS BODIPY mean + SD (*F*) and %7-AAD+ mean + SD values from $n = 3$ replicates of Akata or P3HR-1 BL and GM12879 or GM12881 LCLs grown with or without cystine, Fer-1, and GSH as indicated for 24 h. (*H*) Relative % live cells determined by CellTiter-Glo assay from $n = 3$ replicates of Akata or P3HR-1 BL and GM12879 or GM12881 LCLs grown without cystine across 72 h. *P* values were determined by one-sided Fisher's exact test. $*P < 0.05$, $**P < 0.005$, $***P < 0.0005$.

of NADPH-reducing units and the glycine building block. Indeed, the majority of glutathione synthesized by day 4 postinfection could be traced through EBV-induced mitochondrial one-carbon metabolism (12). Furthermore, human B cells also have higher ratios of oxidized to reduced glutathione than hepatocytes or erythrocytes (50). These results support a model in which EBNA2 and MYC coordinate a redox defense program, increasing one-carbon metabolism to support glutathione biosynthesis needed to suppress ferroptosis while also providing carbon units for de novo purine synthesis (12) (Fig. 7).

EBV induced remarkable sensitivity to BSO at day 2 postinfection, a phenomenon that we did not observe at later time points or with other forms of primary human B cell stimulation. By contrast, many cell types and even cancer cells are resistant to BSO treatment or cystine restriction (46). Yet, EBV-infected cells were sensitive to SLC7A11 and GPX4 blockade at day 2 and also at multiple later time points. We suspect that BSO engaged its GCLC target as it highly induced lipid ROS at day 2, which was suppressed by Fer-1 or GSH supplementation. We favor the hypothesis that day 2 cells are exquisitely sensitive to BSO, as viral transformation converts quiescent B cells into a highly metabolically active state in preparation for Burkitt-like B cell hyperproliferation. Notably, EBNA2 and EBNA-LP are expressed at particularly high levels at day 2 postinfection, which in turn hyper-induce MYC (11, 12, 51). MYC levels are higher in newly EBV-infected cells and in Burkitt cells than in B cells stimulated by receptor agonists or in LCLs. Such aberrantly and rapidly elevated levels of EBNA2 and MYC may therefore create the acute BSO vulnerability at this time point as B cell metabolism swiftly transitions from a quiescent to a highly activated state. It is also possible that BSO did not completely block GCLC activity at the dose used and that even a partial inhibition at day 2 at a dose near the BSO IC_{50} was sufficient to trigger the observed massive lipid ROS and ferroptosis phenotypes given the supply/demand imbalance at this transition point. At later time points, we speculate that there is sufficient glutathione reserve for the cells to buffer BSO effects over the relatively short time of BSO treatment used in our assay and that we therefore did not observe increased lipid ROS or cell death with BSO treatment (Fig. 5 *B* and *C*).

We also note that glutathione has important roles in iron–sulfur [Fe–S] cluster biogenesis. [Fe–S] clusters are highly sensitive to inactivation by ROS and play key roles in mitochondrial metabolism, including in the tricarboxylic acid cycle and oxidative phosphorylation (OXPHOS). The need to rapidly synthesize [Fe–S] clusters at day 2 postinfection may render this time point particularly sensitive to BSO treatment. The resulting perturbation to [Fe–S] clusters, tricarboxylic acid cycle, and OXPHOS may cause reductive stress, adding to cytotoxic effects at this time point.

Profiling studies have revealed a wide range of susceptibility to ferroptosis induction across human cancer cell lines, including B cell lymphomas, yet the basis for this important observation remains to be fully elucidated (30). It is therefore notable that Burkitt cells have low glutathione stores and limited capacity for cystine uptake (52), which may render them exquisitely sensitive to ferroptosis-inducing agents. Our results suggest that glutathione abundance may link the observed sensitivities to SLC7A11 and GCLC inhibition in newly infected and Burkitt cells. Interestingly, we observed that latency III alters ferroptosis sensitivity even within the same cell context. Latency III MUTU and Jijoye Burkitt cells were more refractory to erastin or ML-210 than their latency I counterparts, and P493-6 cells

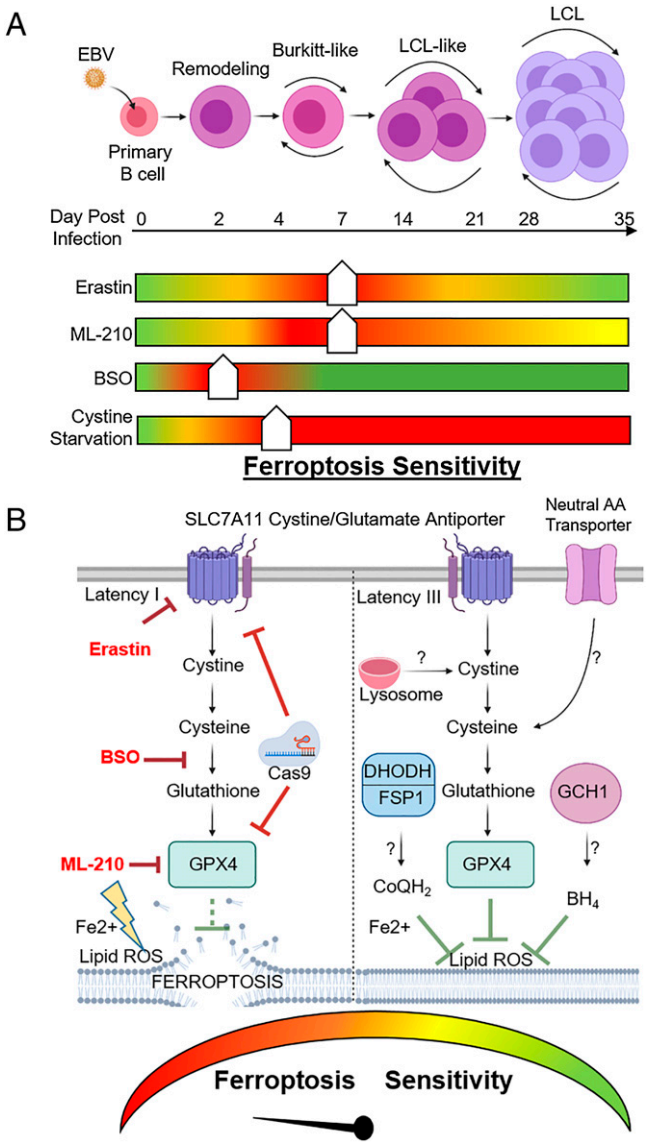

Fig. 7. Model of EBV effects on B cell vulnerability to ferroptosis. (*A*) Schematic of vulnerability to ferroptosis induction at distinct states of EBV-mediated B cell transformation. Ferroptometer sliders demarcate the relative sensitivity of EBV-infected cells to ferroptosis induction to the indicated agent, with green and red indicating the lowest and highest sensitivities to ferroptosis induction, respectively. (*B*) Schematic of vulnerability to ferroptosis-inducing agents in latency I (*Left*) versus III (*Right*) EBV-transformed B cells. Question marks indicate potential pathways by which latency III cells may differentially acquire cysteine and buffer lipid ROS for redox defense.

were more resistant to these agents when grown in the Burkitt-like than in the LCL state. Likewise, we found that EBV-infected cells became more refractory to these agents at later time points of infection as primary cells undergo lymphoblastoid transformation and express latency III. We speculate that latency III–driven increases in glutathione reservoirs contribute to these phenotypes.

Latency III may further alter sensitivity to ferroptosis through additional possible mechanisms (Fig. 7). In particular, latency III may utilize recently described glutathione-independent systems that detoxify lipid ROS in parallel with GPX4 (53). For instance, the oxidoreductase ferroptosis suppressor protein 1 (FSP1, also called AIFM2) reduces ubiquinone (also called coenzyme Q or CoQ) to ubiquinol ($CoQH_2$) at the plasma membrane. $CoQH_2$ can then trap and detoxify

lipid peroxyl radicals independently of GPX4. Similarly, the de novo pyrimidine synthesis enzyme dihydroorotate dehydrogenase (DHODH) generates $CoQH_2$, which can be used to quench lipid ROS within the mitochondrial inner membrane (54). We recently identified that EBV highly induces DHODH and de novo pyrimidine activity in newly infected B cells (55). Furthermore, GTP cyclohydrolase 1 (GCH1) can suppress ferroptosis via the generation of the radical-trapping antioxidant tetrahydrobiopterin (BH4) (56). The use of these ferroptosis-suppressing pathways could potentially explain decreased latency III cell sensitivity to SLC7A11, GCLC, and GPX4 inhibition. It will therefore be of interest to test putative ferroptosis-resistance roles of these recently described pathways in latency III cells.

Cysteine availability is the rate-limiting step in glutathione biosynthesis (57). Cystine is synthesized and released by the liver and is present at ∼50 μM extracellular fluid. It can then be imported by SLC7A11, whereas cysteine, which is present at low concentrations extracellularly, can be imported via neutral amino acid transporters. Our results suggest that the route of B cell stimulation or transformation dictate specific roles of cystine/cysteine import, glutathione synthesis, and GPX4. RNA sequencing data suggest that SLC7A11 is already up-regulated by 2 d post-EBV infection and reaches progressively higher levels at later times as cells transform to the lymphoblastoid physiology (11, 58). Thus, EBV may increase demand for cystine import through SLC7A11, particularly during Burkitt-like hyperproliferation in which lipid biosynthetic pathways may be maximally induced. We suspect that, particularly at later time points, EBV-infected primary B cells may also utilize other neutral amino acid transporters to acquire cysteine. For instance, the Alanine-Serine-Cysteine Transporters 1 and 2 (ASCT1 and 2) are highly induced by EBV (12). Autophagy also has a critical role in early EBV-driven B cell hyperproliferation in the context of metabolic stress (28). Latency III cells may utilize autophagy and perhaps also pinocytosis to acquire lysosomal cysteine, which can then be pumped into the cytosol via the cystinosin lysosomal membrane transporter. Additionally, latency III may increase de novo cysteine synthesis through the transsulfuration pathway, reducing the demand for imported cystine.

We observed significant increases in cell death upon erastin treatment through day 28 postinfection (Fig. 2*B*), albeit with the greatest magnitude within the first week of infection. We speculate that sensitivity is greatest at earlier time points in which cells must import cystine to rapidly synthesize GSH, given our recent finding that EBV highly induces glutathione synthesis in newly infected cells (12). By contrast, we observed robust induction of cell death upon cystine withdrawal at nearly all time points in Fig. 6*B*, which was partially rescuable by Fer-1. The withdrawal of cystine from the media blocks all routes of import and thereby may affect viability at all time points. It is also notable that cystine withdrawal affects the extracellular and intracellular redox states and that this could have contributed to the observed effects on cell viability in a manner distinct from erastin effects on cystine import. Effects on redox states may also impair parallel redox defense pathways, including the antioxidant FSP1, DHODH, and GCH1 pathways, thereby potentially explaining the stronger effect of cystine withdrawal than erastin at late time points of EBV B cell infection and over prolonged periods in LCLs.

Current approaches for BL therapy rely on high-intensity chemotherapy and cause considerable side effects. Therefore, leveraging ferroptosis tumor suppressor roles may offer a promising novel approach. Encouragingly, little acute toxicity has been observed in mouse models with ferroptosis-inducing agents (59). Lower cellular glutathione concentrations increase the cytotoxicity of cyclophosphamide (60), which is used in chemotherapy regimens for BL. It would be of interest to determine whether erastin or ML-210 are synergistic with cyclophosphamide in Burkitt cells. Given the sensitivity of newly infected B cells during Burkitt-like hyperproliferation to ferroptosis-inducing agents, such strategies might also prove useful in preventing the polyclonal outgrowth of newly EBV-infected B cells during high-risk periods, including post-organ transplantation into EBV seronegative hosts in which high rates of post-transplant lymphoproliferative disease are a major clinical challenge. While GPX4 inhibitors suitable for human translational approaches remain to be developed, our results highlight the kinase PSTK as a potentially druggable target for the development of novel ferroptosis-inducing agents.

Materials and Methods

B95.8 EBV Preparation, Primary B Cell Infection and Stimulation. B95-8 EBV was prepared as described (61, 62). EBV titer was determined by a transformation assay. Freshly isolated, deidentified, discarded CD19+ peripheral blood B cells obtained under our hospital institution review board–approved protocol were seeded in Roswell Park Memorial Institute (RPMI) 1640 media supplemented with 10% fetal bovine serum (FBS; one million cells/mL) for infection or stimulation studies. An EBV multiplicity of infection of 0.1 was used, or cells were stimulated by Mega CD40L (50 ng/mL), αIgM (1 μg/mL), CpG (1 μM), and IL-4 (20 ng/mL). For 96 h stimulation, agonists were refreshed at 48 h. Cells were cultured in a humidified chamber at 37 °C in RPMI/10% FBS.

Primary B Cell Isolation and Culture. RosetteSep and EasySep negative isolation kits (Stemcell Technologies) were used sequentially to isolate CD19+ B cells by negative selection, with the following modifications made to the manufacturer's protocols. For RosetteSep, 40 μL antibody mixture was added per mL of blood and before Lymphoprep density medium was underlayed prior to centrifugation. For EasySep, 10 μL antibody mixture was added per mL of B cells followed by 15 μL magnetic bead suspension per mL of B cells. After negative selection, the cells obtained were routinely ≥95% positive for CD19, a nearly pan-B cell surface marker (though not strongly expressed on plasma cells).

CellTiter-Glo. CellTiter-Glo viability assay (Promega) was performed by collecting cells at indicated time points and washing once with 1× PBS. A total of 50 μL cells in PBS were used per assay according to manufacturer instruction.

Software/data Presentation. Graphs were made using GraphPad Prism 7. Schematic models were made using Biorender.

Data Availability. All study data are included in the article and/or *SI Appendix*.

ACKNOWLEDGMENTS. We thank Drs. Vamsi Mootha and Thomas Sommermann for helpful discussions and suggestions. This work was supported by NIH RO1 AI137337, AI164709, and CA228700 and a Burroughs Wellcome Career Award in Medical Sciences to B.E.G., by T32AI007245 to E.M.B. and by T34GM131948 Maximizing Access to Research Careers (MARC) Undergraduate Student Training in Academic Research (U*STAR) program at the University of Rhode Island, Howlett, Niall G. (principal investigator) support for J.V. We thank the Harvard Summer Honors Undergraduate Research Program (SHURP) for support of J.V.

Author affiliations: [a]Division of Infectious Diseases, Department of Medicine, Brigham and Women's Hospital, Boston, MA 02115; [b]Harvard Program in Virology, Harvard Medical School, Boston, MA 02115; [c]Department of Microbiology, Harvard Medical School, Boston, MA 02115; and [d]Broad Institute of Harvard and MIT, Massachusetts Institute of Technology, Cambridge, MA 02142

1. K. W. Wen, L. Wang, J. R. Menke, B. Damania, Cancers associated with human gammaherpesviruses. *FEBS J.*, 10.1111/febs.16206 (2021).
2. C. Münz, Latency and lytic replication in Epstein-Barr virus-associated oncogenesis. *Nat. Rev. Microbiol.* **17**, 691–700 (2019).
3. Y. Pei, A. E. Lewis, E. S. Robertson, Current progress in EBV-associated B-cell lymphomas. *Adv. Exp. Med. Biol.* **1018**, 57–74 (2017).
4. L. S. Young, L. F. Yap, P. G. Murray, Epstein-Barr virus: More than 50 years old and still providing surprises. *Nat. Rev. Cancer* **16**, 789–802 (2016).
5. A. Saha, E. S. Robertson, Mechanisms of B-cell oncogenesis induced by Epstein-Barr virus. *J. Virol.* **93**, e00238-19 (2019).
6. C. Shannon-Lowe, A. B. Rickinson, A. I. Bell, Epstein-Barr virus-associated lymphomas. *Philos. Trans. R. Soc. Lond. B Biol. Sci.* **372**, 20160271 (2017).
7. T. C. Frost, B. E. Gewurz, Epigenetic crossroads of the Epstein-Barr virus B-cell relationship. *Curr. Opin. Virol.* **32**, 15–23 (2018).
8. P. J. Farrell, Epstein-Barr virus and cancer. *Annu. Rev. Pathol.* **14**, 29–53 (2019).
9. C. Alfieri, M. Birkenbach, E. Kieff, Early events in Epstein-Barr virus infection of human B lymphocytes. *Virology* **181**, 595–608 (1991).
10. N. Jochner *et al.*, Epstein-Barr virus nuclear antigen 2 is a transcriptional suppressor of the immunoglobulin mu gene: Implications for the expression of the translocated c-myc gene in Burkitt's lymphoma cells. *EMBO J.* **15**, 375–382 (1996).
11. P. Mrozek-Gorska *et al.*, Epstein-Barr virus reprograms human B lymphocytes immediately in the prelatent phase of infection. *Proc. Natl. Acad. Sci. U.S.A.* **116**, 16046–16055 (2019).
12. L. W. Wang *et al.*, Epstein-Barr-virus-induced one-carbon metabolism drives B cell transformation. *Cell Metab.* **30**, 539–555.e11 (2019).
13. P. A. Nikitin *et al.*, An ATM/Chk2-mediated DNA damage-responsive signaling pathway suppresses Epstein-Barr virus transformation of primary human B cells. *Cell Host Microbe* **8**, 510–522 (2010).
14. D. Pich *et al.*, First days in the life of naive human B lymphocytes infected with Epstein-Barr virus. *mBio* **10**, e01723-19 (2019).
15. L. W. Wang *et al.*, Epstein-Barr virus subverts mevalonate and fatty acid pathways to promote infected B-cell proliferation and survival. *PLoS Pathog.* **15**, e1008030 (2019).
16. R. Schmitz, M. Ceribelli, S. Pittaluga, G. Wright, L. M. Staudt, Oncogenic mechanisms in Burkitt lymphoma. *Cold Spring Harb. Perspect. Med.* **4**, a014282 (2014).
17. L. M. Boxer, C. V. Dang, Translocations involving c-myc and c-myc function. *Oncogene* **20**, 5595–5610 (2001).
18. A. M. Price *et al.*, Analysis of Epstein-Barr virus-regulated host gene expression changes through primary B-cell outgrowth reveals delayed kinetics of latent membrane protein 1-mediated NF-κB activation. *J. Virol.* **86**, 11096–11106 (2012).
19. L. W. Wang, S. Jiang, B. E. Gewurz, Epstein-Barr virus LMP1-mediated oncogenicity. *J. Virol.* **91**, e01718-16 (2017).
20. A. Kieser, K. R. Sterz, The latent membrane protein 1 (LMP1). *Curr. Top. Microbiol. Immunol.* **391**, 119–149 (2015).
21. L. L. Stunz, G. A. Bishop, Latent membrane protein 1 and the B lymphocyte-a complex relationship. *Crit. Rev. Immunol.* **34**, 177–198 (2014).
22. K. H. Shair, N. Raab-Traub, Transcriptome changes induced by Epstein-Barr virus LMP1 and LMP2A in transgenic lymphocytes and lymphoma. *mBio* **3**, e00288-12 (2012).
23. K. Fish *et al.*, Rewiring of B cell receptor signaling by Epstein-Barr virus LMP2A. *Proc. Natl. Acad. Sci. U.S.A.* **117**, 26318–26327 (2020).
24. R. M. DeKroon, H. P. Gunawardena, R. Edwards, N. Raab-Traub, Global proteomic changes induced by the Epstein-Barr virus oncoproteins latent membrane protein 1 and 2A. *mBio* **9**, e00959-18 (2018).
25. A. M. Price, J. E. Messinger, M. A. Luftig, c-Myc represses transcription of Epstein-Barr virus latent membrane protein 1 early after primary B Cell Infection. *J. Virol.* **92**, e01178-17 (2018).
26. M. Hulse, S. M. Johnson, S. Boyle, L. B. Caruso, I. Tempera, Epstein-Barr virus-encoded latent membrane protein 1 and B-cell growth transformation induce lipogenesis through fatty acid synthase. *J. Virol.* **95**, e01857-20 (2021).
27. Z. Lin, J. Liu, R. Kang, M. Yang, D. Tang, Lipid metabolism in ferroptosis. *Adv Biol (Weinh)* **5**, e2100396 (2021).
28. K. McFadden *et al.*, Metabolic stress is a barrier to Epstein-Barr virus-mediated B-cell immortalization. *Proc. Natl. Acad. Sci. U.S.A.* **113**, E782–E790 (2016).
29. B. Gruhne *et al.*, The Epstein-Barr virus nuclear antigen-1 promotes genomic instability via induction of reactive oxygen species. *Proc. Natl. Acad. Sci. U.S.A.* **106**, 2313–2318 (2009).
30. W. S. Yang *et al.*, Regulation of ferroptotic cancer cell death by GPX4. *Cell* **156**, 317–331 (2014).
31. S. J. Dixon *et al.*, Ferroptosis: An iron-dependent form of nonapoptotic cell death. *Cell* **149**, 1060–1072 (2012).
32. B. R. Stockwell *et al.*, Ferroptosis: A Regulated cell death nexus linking metabolism, redox biology, and disease. *Cell* **171**, 273–285 (2017).
33. Z. Shi, N. Naowarojna, Z. Pan, Y. Zou, Multifaceted mechanisms mediating cystine starvation-induced ferroptosis. *Nat. Commun.* **12**, 4792 (2021).
34. G. Xu, H. Wang, X. Li, R. Huang, L. Luo, Recent progress on targeting ferroptosis for cancer therapy. *Biochem. Pharmacol.* **190**, 114584 (2021).
35. J. D. Phelan *et al.*, A multiprotein supercomplex controlling oncogenic signalling in lymphoma. *Nature* **560**, 387–391 (2018).
36. S. Dolma, S. L. Lessnick, W. C. Hahn, B. R. Stockwell, Identification of genotype-selective antitumor agents using synthetic lethal chemical screening in engineered human tumor cells. *Cancer Cell* **3**, 285–296 (2003).
37. G. Miotto *et al.*, Insight into the mechanism of ferroptosis inhibition by ferrostatin-1. *Redox Biol.* **28**, 101328 (2020).
38. J. Muri, H. Thut, G. W. Bornkamm, M. Kopf, B1 and marginal zone B cells but not follicular b2 cells require Gpx4 to prevent lipid peroxidation and ferroptosis. *Cell Rep.* **29**, 2731–2744.e4 (2019).
39. J. A. Bittker *et al.*, "Screen for RAS-selective lethal compounds and VDAC ligands – Probe 2" in *Probe Reports from the NIH Molecular Libraries Program* (NCBI, Bethesda, MD, 2010).
40. I. Ingold *et al.*, Selenium utilization by GPX4 is required to prevent hydroperoxide-induced ferroptosis. *Cell* **172**, 409–422.e21 (2018).
41. A. Tsherniak *et al.*, Defining a cancer dependency map. *Cell* **170**, 564–576.e16 (2017).
42. S. Chiba, Y. Itoh, S. Sekine, S. Yokoyama, Structural basis for the major role of O-phosphoseryl-tRNA kinase in the UGA-specific encoding of selenocysteine. *Mol. Cell* **39**, 410–420 (2010).
43. C. D. Gregory, M. Rowe, A. B. Rickinson, Different Epstein-Barr virus-B cell interactions in phenotypically distinct clones of a Burkitt's lymphoma cell line. *J. Gen. Virol.* **71**, 1481–1495 (1990).
44. G. Habeshaw, Q. Y. Yao, A. I. Bell, D. Morton, A. B. Rickinson, Epstein-Barr virus nuclear antigen 1 sequences in endemic and sporadic Burkitt's lymphoma reflect virus strains prevalent in different geographic areas. *J. Virol.* **73**, 965–975 (1999).
45. M. Schuhmacher *et al.*, The transcriptional program of a human B cell line in response to Myc. *Nucleic Acids Res.* **29**, 397–406 (2001).
46. C. D. Poltorack, S. J. Dixon, Understanding the role of cysteine in ferroptosis: Progress & paradoxes. *FEBS J.* **289**, 374–385 (2022).
47. D. Metcalf, Role of mercaptoethanol and endotoxin in stimulating B lymphocyte colony formation in vitro. *J. Immunol.* **116**, 635–638 (1976).
48. E. L. Pearce, M. C. Poffenberger, C. H. Chang, R. G. Jones, Fueling immunity: Insights into metabolism and lymphocyte function. *Science* **342**, 1242454 (2013).
49. M. Akkaya *et al.*, Second signals rescue B cells from activation-induced mitochondrial dysfunction and death. *Nat. Immunol.* **19**, 871–884 (2018).
50. M. H. Falk *et al.*, Apoptosis in Burkitt lymphoma cells is prevented by promotion of cysteine uptake. *Int. J. Cancer* **75**, 620–625 (1998).
51. B. Kempkes, P. D. Ling, EBNA2 and its coactivator EBNA-LP. *Curr. Top. Microbiol. Immunol.* **391**, 35–59 (2015).
52. A. Banjac *et al.*, The cystine/cysteine cycle: A redox cycle regulating susceptibility versus resistance to cell death. *Oncogene* **27**, 1618–1628 (2008).
53. B. Gan, Mitochondrial regulation of ferroptosis. *J. Cell Biol.* **220**, e202105043 (2021).
54. C. Mao *et al.*, DHODH-mediated ferroptosis defence is a targetable vulnerability in cancer. *Nature* **593**, 586–590 (2021).
55. J. H. Liang *et al.*, Epstein-Barr virus induced cytidine metabolism roles in transformed B-cell growth and survival. *mBio* **12**, e0153021 (2021).
56. V. A. N. Kraft *et al.*, GTP cyclohydrolase 1/tetrahydrobiopterin counteract ferroptosis through lipid remodeling. *ACS Cent. Sci.* **6**, 41–53 (2020).
57. T. Ishii, Y. Sugita, S. Bannai, Regulation of glutathione levels in mouse spleen lymphocytes by transport of cysteine. *J. Cell. Physiol.* **133**, 330–336 (1987).
58. C. Wang *et al.*, RNA sequencing analyses of gene expression during Epstein-Barr virus infection of primary B lymphocytes. *J. Virol.* **93**, e00226-19 (2019).
59. Y. Zhang *et al.*, Imidazole ketone erastin induces ferroptosis and slows tumor growth in a mouse lymphoma model. *Cell Chem. Biol.* **26**, 623–633.e9 (2019).
60. F. Y. Lee, D. J. Flannery, D. W. Siemann, Prediction of tumour sensitivity to 4-hydroperoxycyclophosphamide by a glutathione-targeted assay. *Br. J. Cancer* **63**, 217–222 (1991).
61. M. A. Calderwood, A. M. Holthaus, E. Johannsen, The Epstein-Barr virus LF2 protein inhibits viral replication. *J. Virol.* **82**, 8509–8519 (2008).
62. E. Johannsen *et al.*, Proteins of purified Epstein-Barr virus. *Proc. Natl. Acad. Sci. U.S.A.* **101**, 16286–16291 (2004).